Experimental measurements of the RF sheath thickness with a cylindrical Langmuir probe

E Faudot, J Ledig, J Moritz, S Heuraux, N Lemoine, S Devaux

Experimental measurements of the RF sheath thickness with a cylindrical Langmuir probe

Cite as: Phys. Plasmas **26**, 083503 (2019); https://doi.org/10.1063/1.5096018
Submitted: 14 March 2019 . Accepted: 15 July 2019 . Published Online: 08 August 2019

E. Faudot, J. Ledig, J. Moritz, S. Heuraux, N. Lemoine, and S. Devaux

Physics of Plasmas ARTICLE scitation.org/journal/php

Experimental measurements of the RF sheath thickness with a cylindrical Langmuir probe

Cite as: Phys. Plasmas **26**, 083503 (2019); doi: 10.1063/1.5096018
Submitted: 14 March 2019 · Accepted: 15 July 2019 ·
Published Online: 8 August 2019

E. Faudot,[1] J. Ledig,[1] J. Moritz,[1] S. Heuraux,[1] N. Lemoine,[1] and S. Devaux[1,2]

AFFILIATIONS

[1]Institut Jean Lamour, Campus Artem, 2 allee André Guinier, 54011 Nancy, France
[2]CRYOSCAN, Campus Artem, 2 allee André Guinier, 54011 Nancy, France

ABSTRACT

The small layer oscillating in front of a radio frequency (rf) biased electrode in an asymmetric rf plasma discharge without a magnetic field is diagnosed using an rf compensated cylindrical probe. Thanks to this probe (0.15 mm in diameter), the floating potential is measured in this area. Radio frequency plasmas and sheath properties are then derived from the I-V characteristics measured by the probe at different rf power levels in both capacitive and direct couplings. In direct coupling, the plasma biasing is, as expected, nearly equal to the applied rf potential except at high power levels for which the current collected by the electrode saturates and the sheath potential gap is reversed. In capacitive coupling, the self-biasing of the electrode is strongly negative due to the matching box used. From the difference between the plasma potential and the floating potential, we found a sheath thickness of about 3 λ_{De}. Within the rf power scan performed, the sheath thicknesses deduced from the potential and density profiles are 3 times higher than those from the Child–Langmuir law both in direct and capacitive coupling in a low collisional helium plasma.

I. INTRODUCTION

Diagnosing radio frequency (rf) plasmas is a rather complicated task even without a magnetic field, and the study of rf sheaths by probes is still a challenge even if rf discharges have been deeply studied.[1] In the literature, one can find out the main characteristics of an unmagnetized rf plasma discharge, collisional or not, symmetric or asymmetric, in direct or capacitive coupling. Lieberman and Lichtenberg[2] and Chabert and Braithwaite[3] described the main characteristics of rf discharges, especially the rf sheath which is characterized by a typical thickness, capacitance, and resistance. One of the first to investigate rf sheath properties is Godyak[4] whose numerous works have modeled and measured the sheath thickness and capacitance.

The main consequence of the oscillating sheath close to an rf electrode is the self-biasing either of the electrode itself in the case of a capacitive coupling or of the plasma itself in direct coupling. By allowing dc current to flow through the electrode (direct coupling) or not leads to a very different type of biasing which in turn modifies the sputtering. This biasing comes from the rectification of the rf potential by the sheath, due to the nonlinearity of its capacitance and conductance.[5] This nonlinear response is simply given by the Boltzmann density distribution for an electron in a collisionless sheath.

The sheath is a thin space charged layer that can be defined by its typical thickness and the voltage drop between its edge and wall, which can be biased (dc or rf sheath) or nonbiased (floating sheath). The sheath edge, or its thickness, is defined through the Bohm criterion which is fulfilled when the ion velocity is larger than the acoustic speed at the sheath edge. This criterion has been refined by Ref. 6, but no simple analytical solution really exists for the sheath thickness, except for the well-known Child–Langmuir law, which provides the sheath width as a function of the sheath potential (much higher than the floating potential) with no collision.[3] For the case of a floating sheath, the reader should refer to Ref. 7 in which the thickness is calculated from a fluid model and leads to an approximate sheath width of 5 λ_{De}, where λ_{De} is the Debye length.

In the context of an rf discharge, many models have been developed: collisionless[8] and collisional sheath[9] as well as an improved fluid model with arbitrary collision parameters.[10] These models provide the main properties of the sheath: conductance, capacitance, thickness, and average potential drop as a function of the rf potential. The latest numerical calculations seem to show that the rf sheath thickness is much larger than the one given by the Child–Langmuir law.[11] Other models are more suitable to calculate the time averaged rf sheath potential in asymmetric capacitive rf discharges[12,13] or in the case of the instantaneous rectified potential.[14–16] The model presented in Ref. 14 is also valid with direct current (blocking capacitor short circuited). In the case of an asymmetric rf discharge with direct coupling, an exact solution of the instantaneous rf sheath potential as a function of the areas and capacitances of both sheaths is given in Ref. 17 in which an asymmetric double probe model with capacitive rf currents is used.

Other attempts to measure the sheath thickness have already been made, but they used different methods in different plasmas. A review of the main ways to diagnose the sheath (dc and rf) is given in Ref. 18. The first observation of the sheath width was made by Langmuir in mercury discharges. One of the main contributors in the field is Godyak and Sternberg[10] who provided a very complete model for the sheath capacitance and thickness, corroborated by measurements. These measurements, also performed in a mercury vapor plasma in a symmetric rf discharge, consisted of measuring the sheath capacitance to deduce the sheath thickness. Another method uses emissive probes to measure directly the plasma potential in the dc sheath[19] and rf sheath[20] in a multidipole plasma and at low frequencies (lower than 1 MHz). A third method is based on the laser detachment signal and is compared with probe measurements and the Child–Langmuir law.[21] These measurements were performed in a weakly magnetized plasma around a cylindrical biased probe. A fourth method consists of measuring the electric field in a rf sheath thanks to an electron beam probe in a rf parallel plate capacitive discharge in an argon plasma.[22] Recently, Han *et al.*[23] retrieved the sheath width from the collected ion current on a cylindrical probe surface.

Langmuir probe theory is still mainly based on the first paper from Langmuir[24] who first described the currents collected by different kinds of biased probes (plane, cylindrical, and spherical) in a potential well: the Orbital Motion Limit (OML) theory. Other theories have then been elaborated by many authors leading to the Allen-Boyd-Reynolds (ABR)[25] theory. This theory is dedicated to spherical probes and extended to cylindrical probes.[26] One can also cite the Bernstein-Rabinowitz[27] theory for monoenergetic ions, refined by Laframboise,[28] but it is much more complex to apply. Another method just takes into account the sheath expansion theory[29] to calculate the true collecting area of the probe. Our rf compensated[30] cylindrical probe was manufactured by the Hiden Company and automatized by the Cryoscan company. The rf compensation has been changed to compensate frequencies from 25 to 60 MHz. Nevertheless, the choice of chokes to cut off rf currents must be done carefully to be really efficient.[31]

Our experimental setup, plasma chamber, rf electrode, and probe are described in Sec. I. Section II is dedicated to probe the measurements and the methods used to deduce the plasma parameters from the current-voltage (I-V) characteristics. Section III deals with the experimental results and presents potential profiles inside and outside the rf sheath. Section VI is dedicated to the comparison of the measured and theoretical sheath thicknesses with different techniques to find out the sheath edge.

II. EXPERIMENTAL SETUP

All measurements were performed in the linear experimental device Aline[32] depicted in Fig. 1. It is a cylindrical chamber of length 1 m and diameter 30 cm surrounded by 6 axial coils capable of producing a maximum of 0.12 T magnetic field (in the frame of the present paper, the plasma is not magnetized). It is also equipped with a 600 W broadband (from 10 kHz to 250 MHz) RF amplifier driven by a frequency synthetizer. Such an RF amplifier is usually used in RF antenna applications for telecommunications. Here, it is connected to the RF electrode (a stainless steel disk of diameter 8 cm and thickness 1 cm, as shown in Fig. 3) via a RF coupler to measure both forward and reflected power and via a matching box to match at frequencies from 10 to 40 MHz, depending on the plasma discharge parameters. The amplifier is also protected against reflected power up to 400 W. In addition, a 3 axis manipulator developed by Cryoscan holds the Langmuir probe. It can move by ± 5 cm along the x and y axes (radial) and by 50 cm along the z axis (axial). This allows us to build potential profiles in the plasma or even 3D maps.[45] The probe acquisition system, the manipulator, the frequency synthetizer, and the oscilloscope are all driven by single software in order to control all the instruments and at the same time to automatize the acquisition. As a matter of fact, the manual operation would require too much time according to the many parameters to control: power and frequency (synthetizer) I-V characteristics (probe), probe position (manipulator), and even magnetic field strength in the case of magnetized plasmas. The gas pressure is 3.4 Pa for all the discharges presented here.

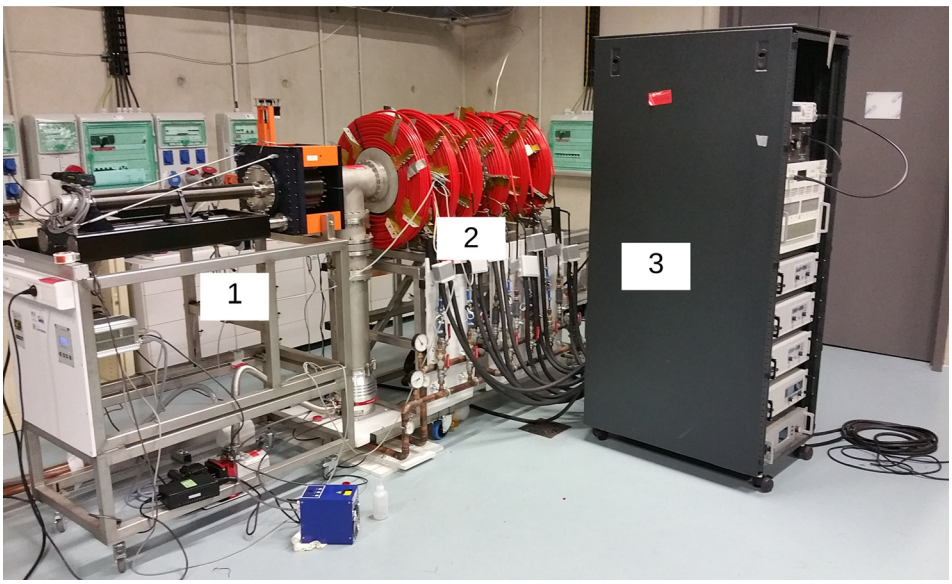

FIG. 1. Picture of the Aline device. The 3D manipulator (1) in which the probe arm is mounted is connected to the vacuum chamber (2) and the turbo pump. The magnetic red coils are connected to the 3 power dc supplies [bottom of (3)], while the rf electrode is connected to the rf amplifier [in the middle of (3)].

A. Capacitive and direct coupling

Two choices are possible to perform RF plasma discharges. The first consists in direct coupling (see Fig. 2), where the amplifier is directly connected to the electrode via the coupler. The second one is capacitive coupling, where a matching box is inserted between the coupler and the electrode to avoid reflected power to the amplifier and hence increase the power efficiency. These couplings lead to very different types of biasings of the plasma discharges as it is explained in the Raizer book.[1] In direct coupling, the DC current is allowed and the averaged (over one RF period) potential on the electrode is zero, while the averaged plasma potential is biased at a fraction of the RF potential depending on the asymmetry of the discharge:[17] this ratio varies in the range of $1/\pi$ to 1. In capacitive coupling, DC currents are not allowed, only displacement currents are, so that the electrode is negatively biased to equal the electron flux to the ion one. Since this means that almost all the electrons are repelled, the negative bias on the electrode is close to the RF potential peak amplitude.

In the present work, the RF power has been scanned from −16 dBm to −5 dBm per step of −1 dBm. The RF amplifier increases this signal by 57 dBm (±1 dBm) according to the frequency, which leads to a power scan from 12 W to 160 W. Both types of couplings have been tested and presented in Secs. IV B and IV C.

B. The probe

The main diagnostics available is an RF compensated Langmuir probe from the Hiden Company.[30] This probe has a cylindrical tip of length 1 cm and diameter 0.15 mm as depicted in Fig. 3. It is equipped with a compensation electrode and with small inductors able to cut off RF currents at their resonant frequencies which have been chosen according to the working frequencies (between 25 and 40 MHz). It can be noticed that both the 1st and 2nd harmonics of the RF frequency must be compensated due to potential rectification by the sheath. The RF compensation is essential for measuring the real temperature and floating potential because RF currents can distort the I-V characteristics as shown in Fig. 4. These I-V characteristics are plotted according to the following equation:[17]

$$I_p = S_1 j_i \left\langle \frac{\exp(\phi_{rf}) - \exp(\phi_p)}{\exp(\phi_{rf}) + S_1/S_2 \exp(\phi_p)} \right\rangle, \quad (1)$$

with j_i being the ion saturation current density, $\phi_{rf} = 10 + \frac{V_{rf}}{T_e}\sin(\omega t)$, V_{rf} the rf potential amplitude, S_1 the probe area, S_2 the wall area, and $\phi_p = V_p/T_e$ the probe potential. T_e is here expressed in eV. Usually, $S_2 \gg S_1$ and thus the current can be expressed as a simple sheath current, while if $S_1 = S_2$, the current becomes a tanh function of the rf potential. The plotted I-V characteristic is averaged over one RF period.

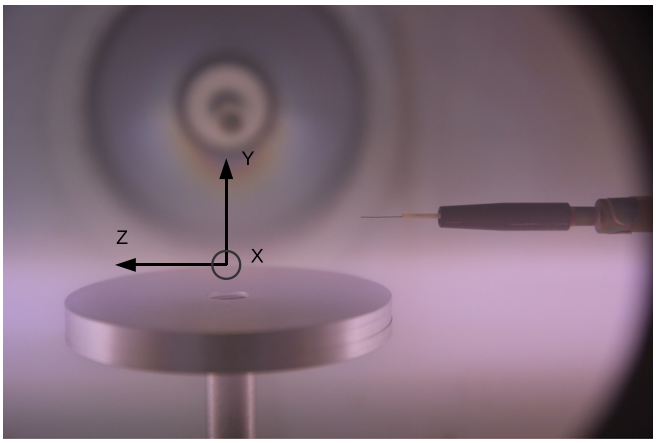

FIG. 3. Picture of the probe and the RF electrode.

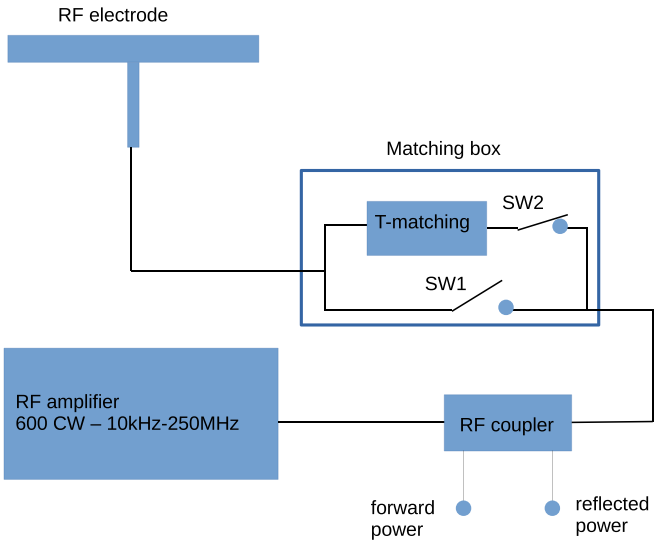

FIG. 2. Sketch of the amplifier connected to the RF electrode. Between them, the RF coupler is used to measure both forward and reflected power, and the matching box can either be shunt by switch 1 (direct coupling) or used as a T matching with switch 2 (capacitive coupling).

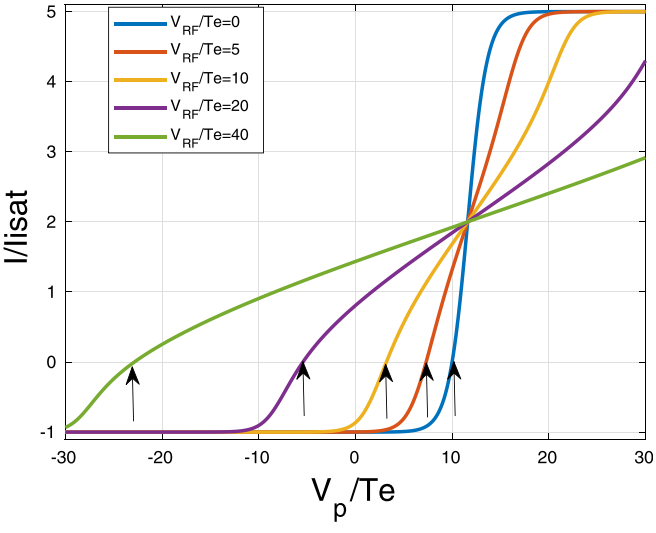

FIG. 4. Uncompensated I–V characteristics for different RF potentials.

III. I-V CHARACTERISTICS

The I-V characteristics have been treated according to 2 different methods. The first is a fit of the ion and exponential part of the characteristics (as explained in Sec. IV), and the second is based upon the OML theory. But the primary condition to make the characteristics usable is the low level of current noise when sweeping the voltage on the probe. The probe voltage is swept from −70 to +70 V by a 0.02 V step at an acquisition frequency of 65 kHz. Each presented IV characteristic has been averaged 20 times to lower the noise, leading to high quality signals which are able to be derived without too many uncertainties. Several I-V characteristics are plotted in Fig. 5, each of them corresponding to a y position (see Fig. 3) between −5 and +35 mm per 1 mm step. The electrode upper edge is at y = −7 mm for this measurement.

A. Fit of the I-V characteristics

The fit of the ion part and exponential part is a fast method to deduce the ion density n_i, the electron density n_e, and the electron temperature T_e in a single operation. The fit is achieved thanks to a nonlinear method provided in Matlab software able to deduce each free parameter by successive iteration using a least squares method. The advantage of the method is the robustness, while the starting parameters (here n_i, n_e, and T_e) are not too far from the final ones. The fit function [Eq. (2)] takes into account the sheath expansion in the ion part according to the Child–Langmuir law to deduce the size of the sheath surrounding the probe and the classical exponential part for Boltzmann electrons collected by the repelling probe. The probe potential V_p is thus always lower than the plasma potential V_{pl}. The last one is deduced from the maximum of the first derivative of the I-V characteristic with good accuracy (less than 1 V) according to the quality of the IVs which have even been smoothed in a second pass

$$I(V_p) = -I_i - \alpha(V_{pl} - V_p)^{\frac{3}{4}} + I_e \exp\left(-\frac{V_{pl} - V_p}{T_e}\right), \quad (2)$$

$$n_e = I_e.e^{-1.5} Sp^{-1} \sqrt{2\pi m_e / Te}, \quad (3)$$

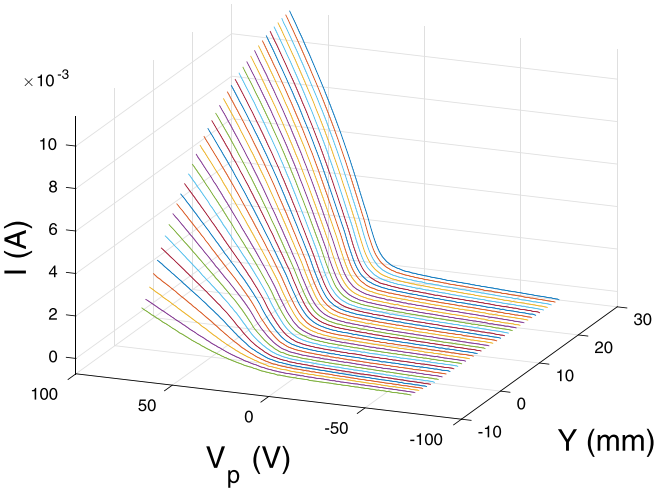

FIG. 5. Averaged I–V characteristics for different positions along the y axis.

$$n_i = \frac{I_i}{eC_s S_p}. \quad (4)$$

I_i and I_e are the ion and electron saturation currents, respectively, S_p is the probe area, m_e is the electron mass, C_s is the ion acoustic speed, and α is a coefficient depending on the sheath expansion around the probe when collecting ions. To check the reliability of the method, one can compare n_i and n_e which should theoretically be equal. In most of the I-V studies, both of them can be very different, a factor 2 or more is often observed. The advantage of this method is that the α coefficient is just a free parameter to fit perfectly the characteristics, but it is not used to deduce any physical parameter, which is suitable according to big uncertainties involved in the sheath expansion.

B. OML theory applied to the I-V characteristics

The classical Orbital Motion Limit (OML) theory has been applied to the ion part using an I^2 method, while the temperature has been deduced from the derivative of the log of the electron current, which means that ion current must first be deduced from a previous temperature evaluation. Next, iterations are performed to converge to the most probable temperature and density. This method has been successfully used in other rf plasma with the same cylindrical probe.[33] In both methods, the floating potential is always at I = 0 and the plasma potential is at the maximum of the first derivative. This OML method is widely documented in Langmuir and Bohm works.[24,34] The advantage of the OML theory is to deduce the ion density from the ion part even when the probe is located inside the sheath, while the fit method applied to the exponential part does not work anymore due to distortion of the I-V characteristics inside the sheath. Of course, the density deduced from OML theory inside the sheath is not a good one because the ion EDF (Energy Distribution Function) is not Maxwellian, but this theory remains good in the plasma up to the sheath edge, and by continuity, a sharp transition in the density can be seen over the sheath edge. In the sheath, ions are accelerated so that the mean velocity is higher. At a constant flux, the ion density should then be lower than the one deduced from the OML theory. But again, the interest is to obtain a continuous density profile to find out the sheath edge, and this can only been done using ion flux.

IV. MEASUREMENTS INSIDE AND OUTSIDE THE rf SHEATH

A. Experimental protocol

This section is dedicated to the analysis of plasma parameters resulting from I-V characteristic processing using both methods. The main goal of these experiments is to measure the potential profile from few centimeters off the rf electrode (outside the rf sheath) to a very small distance (as low as 1 mm) to its surface which is now located at y = 0 mm. According to the typical size of the rf sheath (1 cm), one can even expect a potential profile inside the sheath (1 mm space step). To do so, a position scan has been performed to reconstruct the density profile for each step of the power scan mentioned earlier. This has been done for both rf couplings (capacitive and direct). For each of the 46 positions composing a profile, the I-V characteristic has been recorded. In total, 1104 I-V characteristics have been measured thanks to our automated measurement software

TABLE I. Scan parameters.

Coupling	Direct	Capacitive
rf power scan (dBm)	41:1:52	41:1:52
y position scan (mm)	1:1:46	1:1:46
y electrode position (mm)	0	0
Gas type	He	He
Gas pressure (Pa)	3.4	3.4

controlling the manipulator, the probe, and the RF power at the same time. All parameters are listed in Table I.

B. Potential profiles within the sheath

By plotting the measured floating potential V_{fl} (Figs. 6 and 10) and plasma potential V_{pl} (Figs. 7 and 8) profiles along the y axis, one can measure the sheath thickness and the plasma potential as a function of the rf power in both couplings. The floating potential profiles are easy to determine from the I-V characteristics (at $I = 0$) and exhibit a quasiconstant slope in the presheath (at least 2 cm away from the electrode) and a sudden drop at the sheath edge. The plasma potential profile can be plotted from the maximum of the first derivative of the I-V characteristics outside the sheath. Within the sheath, it tends to strongly increase due to the distortion of the velocity distribution function. This property could also be used to detect the sheath edge.

The classical definitions of the floating and plasma potential are used outside the sheath: the floating potential is the potential of a floating collecting surface at $I = 0$ and the plasma potential is the potential seen by a transparent probe collecting no charge. Within the sheath, both definitions are the same except that the EDF is not a Maxwellian anymore because electrons are repelled, while ions are accelerated. The potential drop $\Delta\phi_{fl}$ between the plasma potential and the floating potential should be maximum at the sheath edge $[j_e(y = s) = j_e]$ and 0 $[j_e(y = 0) = j_i]$ at the rf electrode surface in capacitive coupling according to Eq. (5). In direct coupling, there is a dc current Δj flowing between the rf electrode and the wall. This one is mostly electronic for an rf electrode much smaller than the grounded wall, and thus, the floating potential should be lower than expected. At low current $\Delta j \ll j_e$, the difference should not be visible

$$\Delta\phi_{fl}(y) = \ln\left(\frac{j_i}{j_e(y)}\right). \tag{5}$$

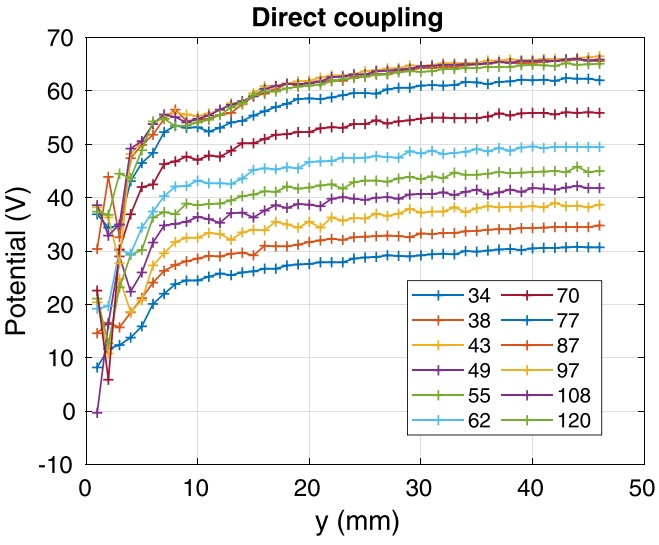

FIG. 6. Floating potential measured by the probe with respect to the position along the y axis in direct coupling for 12 rf potential amplitudes (legend in volts).

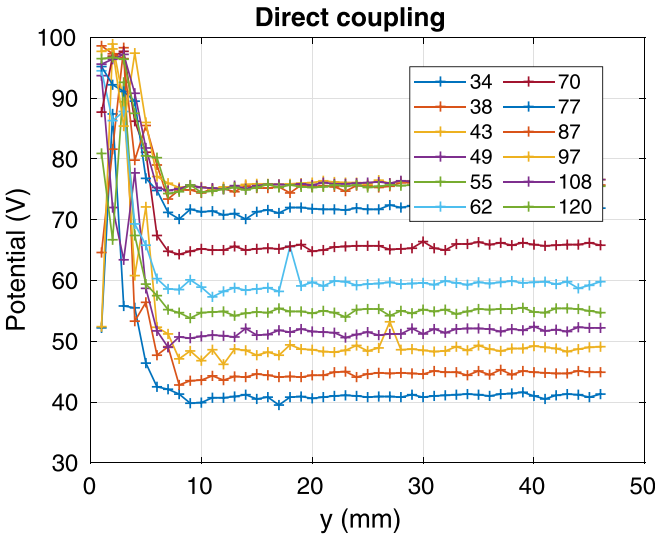

FIG. 7. Plasma potential measured by the probe with respect to the position along the y axis in direct coupling for 12 rf potential amplitudes (legend in volts).

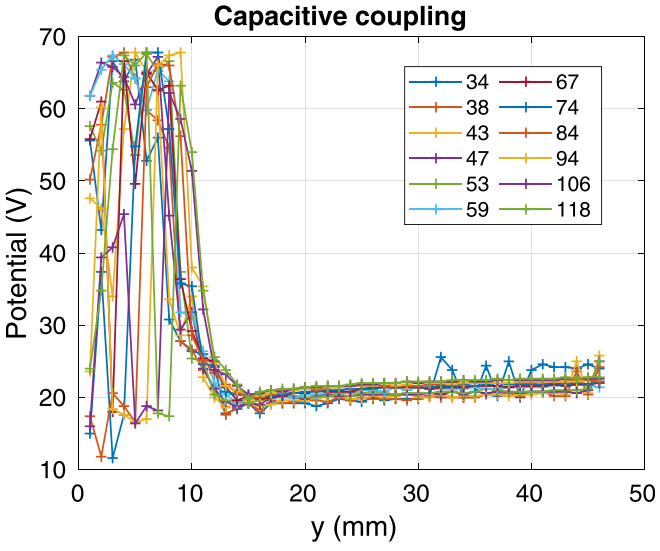

FIG. 8. Plasma potential measured by the probe with respect to the position along the y axis in capacitive coupling for 12 rf potential amplitudes (legend in volts).

1. Direct rf coupling

In direct coupling (Figs. 6 and 7), both floating and plasma potentials increase with the applied rf potential because the averaged potential on the electrode remains at 0 V, while the plasma is biased at a fraction of the rf potential amplitude. One can see that the floating potential does not converge to 0 V due to electrostatic perturbations of the probe within the sheath.[18]

For a symmetric rf discharge, i.e., $S_1 = S_2$, with S_1 being the rf electrode area and S_2 the grounded wall area, and with small rf sheath capacitance, the time averaged plasma potential is $V_{rec} = \Delta V_{fl} + V_{rf}/\pi$[35] with $\Delta V_{fl} = \Delta\phi_{fl}/T_e$ [see Eq. (7)]. For a high capacitive sheath, the averaged plasma potential tends to $V_{sat} = \Delta V_{fl} + V_{rf}$. More sophisticated models have been derived at relatively low frequency[16] and using Bessel functions first applied to Langmuir probes[36] and then to rf discharges.[5,13,37,38] Measurements of the average plasma potential have also been compared with the models[13] in an argon plasma. Between these two regimes, a general formula is given by Eq. (18) in Ref. 17 but the model the most able to fit the measured potential here is the saturated regime given by Eq. (30) in Ref. 45. According to this model, the time average plasma potential is

$$\langle\phi\rangle = \Delta\phi_{fl} + \ln\left(\frac{S_1 I_0(\gamma_2\phi_{rf}) + S_2 I_0(-\gamma_1\phi_{rf})}{S_1 + S_2}\right), \quad (6)$$

$$\Delta\phi_{fl} = -\ln\left(2\pi\frac{m_e}{m_i}\right), \quad (7)$$

where $\gamma_1 = \frac{C_1}{C_1+C_2}$ and $\gamma_2 = \frac{C_2}{C_1+C_2}$, with C_1 and C_2 being the rf sheath capacitance at the electrode and at the wall. It has been shown[17] that this model can also be used for a magnetized flux tube connected to an rf electrode. In that case, the capacitance C_2 is replaced by $C_\perp + C_2$, with $C_\perp$ being the equivalent transverse capacitance of the flux tube exchanging rf currents. It means that both a magnetized flux tube and an asymmetric discharge exhibit the same behavior in the case of a direct coupling.

Applying these equations to experimental measurements, one can see in Fig. 9 that the plasma and floating potentials measured by the probe as a function of rf potential increase almost linearly up to 70 V and then saturate. The linear part of the measured plasma potential curve must be higher than V_{rec} and lower than V_{sat} which are the lowest and highest theoretical values. But it can also be well fitted by Eq. (6) with S_1 being the real electrode area, $S_2 = 3S_1$, which is far from the real wall area (true $S_2 = 100S_1$), and $C_1 = \epsilon_0 S_1/d_1$ and $C_2 = \varepsilon_0 S_2/d_2$ with $d_1 = 5$ mm and $d_2 = 50$ mm. C_1 is close to the true sheath capacitance deduced from the sheath thickness, while C_2 has been adjusted to fit the plasma potential curve. The conclusion of the fit is that the real plasma discharge is far much complex than the model in which the density and plasma potential outside the sheath are considered constant. The rf ionization occurs close to the rf electrode, outside the sheath, because electrons are stochastically heated by the rf sheath.[39] This local heating cannot be seen in the direct coupling profile but will be seen in the capacitive coupling profiles.

Finally, one can check that the gap between plasma and floating potential remains constant at all rf potential values. This gap should be equal to Eq. (7) yielding 17.7 V for $T_e = 5$ eV. Actually, the measured value is 10.8 V, i.e., 7 V lower than expected. This discrepancy can be explained either by a wrong temperature T_e or from the different

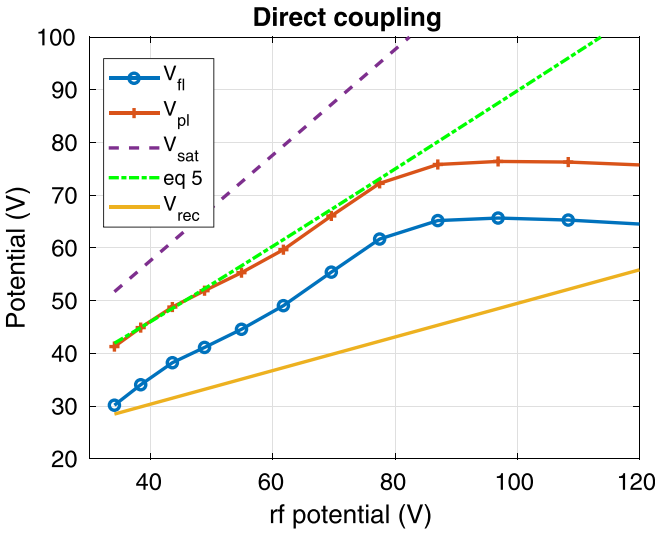

FIG. 9. Floating V_{fl} and plasma V_{pl} potentials measured by the probe with respect to the applied rf potential at the electrode in direct coupling. $V_{rec} = \Delta V_{fl} + V_{rf}/\pi$ and $V_{sat} = \Delta V_{fl} + V_{rf}$.

collecting areas for each species. The deviation in the temperature can be due to a non-Maxwellian electron energy distribution function (EEDF), making an accurate evaluation of the temperature very difficult. But assuming a good temperature, for such a cylindrical probe, the gap can be adjusted from the effective collecting areas for electrons S_e and ions S_i according to the following equation:

$$\Delta\phi_{fl2} = -\ln\left(2\pi\frac{m_e}{m_i}\right) - \ln\left(\frac{S_e}{S_i}\right). \quad (8)$$

Assuming that the ion collecting area is the probe tip surrounded by a 3 λ_{De} thick sheath[7] and the electron collecting area is the actual tip area, the 7 V drop can be explained. We have taken in this calculation the average temperature and densities plotted in Sec. V: $T_e = 5$ eV and $n = 2.5 \times 10^{16}\ m^{-3}$.

The last discussion about the direct coupling potential concerns the saturation of the plasma potential at 70–75 V, while the rf potential still increases. To explain that, one assumes that the electron current at the electrode also saturates, and it can be calculated using Eq. (31) in Ref. 17. Actually, this formula must be corrected because the area $S_1 + S_2$ should appear at the numerator as follows:

$$|I_1| = j_i S_2\left(1 - \frac{S_1 + S_2}{S_1 I_0(\phi_{rf}) + S_2}\right), \quad (9)$$

where I_1 is the current collected by the electrode in the high sheath capacitance regime and I_0 is the modified Bessel function of the first kind. The rf potential limit for the saturation can then be deduced from $|I_1(\phi_{rf})| > I_{esat} = j_e S_1$. Beyond this limit, the electron flux must be accelerated by the sheath in which the potential drop is reversed. Increasing the rf potential increases the sheath voltage as well, but not the plasma potential, which explains the saturation of the plasma potential.[40] From Eq. (9), with S_1 and S_2 being the effective electrode and wall areas, the limit rf potential is equal to 29 V, instead of 80 V in

Fig. 9. This means that the real wall area or the plasma density close to the wall is overestimated as already seen in the fit parameters of Eq. (6). This is not a surprise as the density decreases along the profile. Moreover, formula 9 is only valid for $|I_1| < I_{esat}$. As a consequence, an accurate value of the potential is then not possible to get. Such electron sheaths have already been studied and measured,[18,41,42] where it is shown that the modification of the electrode area is a key parameter to reverse the electric field in the sheath.

2. Capacitive coupling

In capacitive coupling, all the rf potential grows inside the rf sheath due to the negative self-biasing of the rf electrode to repel electrons. This capacitive coupling is ensured by a matching box (T matching) composed of two capacitors and one tunable inductor. The floating potential profiles are almost identical outside the rf sheath. Inside the sheath, the potential gap increases with the rf potential (Fig. 10). The floating potential value close to the rf electrode should be almost equal to the electrode potential as this potential depends on the electron flux arriving onto the probe. Deeper into the sheath, the electron flux decreases, leading to a decrease in the floating potential. Here, the lowest floating potential that can be measured by the probe depends on the first value of the probe potential scan which is −70 V. The floating potential outside the sheath is close to the value given by Eq. (8). Nevertheless, one can see that the higher the rf potential, the deeper the potential well in front of the sheath edge. This well is probably due to electron heating as explained above. This effect is more visible in the present case as the total potential drop in the sheath is much higher than the rf potential because of the matching box. As a matter of fact, the self-biased electrode potential V_{bias} can reach −500 V while the rf potential measured before the matching box is slightly higher than 100 V as shown in Fig. 11.

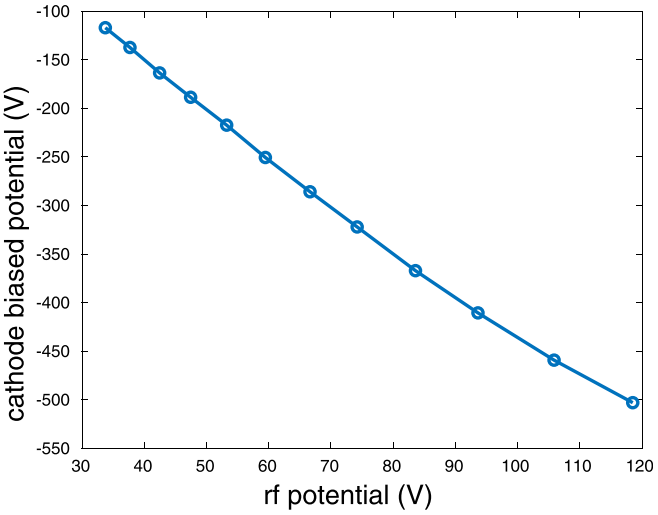

FIG. 11. Amplitude of the dc biased potential at the electrode V_{bias} with respect to the rf potential at the entrance of the matching box (capacitive coupling).

As for the plasma potential profiles (Fig. 8), it is clearly flat outside the sheath, while it increases strongly at the sheath edge. The only way here to retrieve the plasma potential within the sheath is to use an emissive probe.[18] Then, taking the averaged potentials over the last 5 points of the profiles (the farthest from the electrode), one can plot both the plasma and floating potential as a function of the rf potential (see Fig. 12).

The last point is that the potential gap between the plasma and floating potentials is roughly 13 V which is in agreement with Eq. (8) with $T_e = 6$ eV. This gap is constant in the first part of the curve below 80 V for the rf potential. Beyond this value, the potential well extends up to a few centimeters away from the sheath edge and decreases the

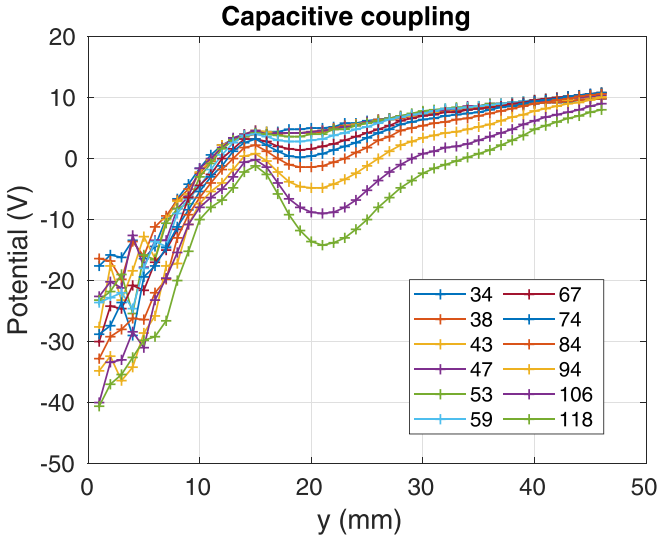

FIG. 10. Floating potential V_{fl} measured by the probe with respect to the position along the y axis in capacitive coupling for 12 rf potential amplitudes (legend in volts).

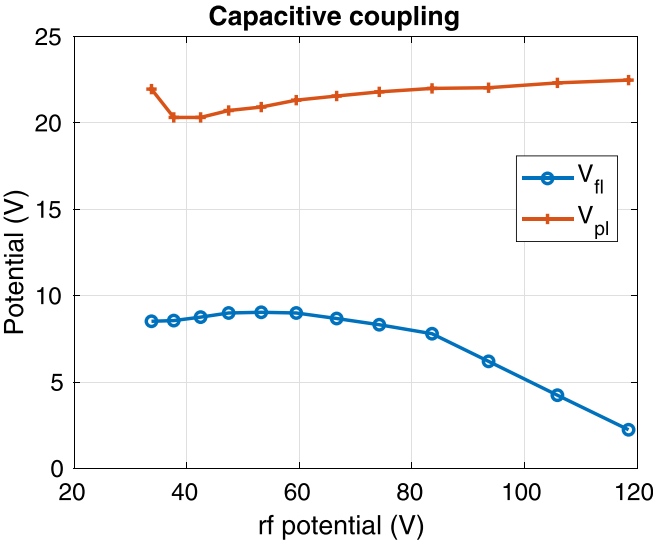

FIG. 12. Floating V_{fl} and plasma V_{pl} potentials measured by the probe with respect to the applied rf potential at the electrode in capacitive coupling.

floating potential due to the increase in T_e in this "heating" region. The typical size of the potential well is of the order of the mean free path for electron-neutral collisions (≈2 cm).

C. Densities and temperatures

For direct coupling and from the fit method, the ion and electron densities are plotted in Fig. 13 and the electron temperature is plotted in Fig. 15. The first remarkable result is the quasisquare root dependence of the density vs the RF power (power 0.6 for n_e and 0.63 for n_i). The second result is the relatively small discrepancy between n_i and n_e with the fit method which takes into account the expansion of the sheath. The average n_i/n_e ratio is equal to 1.34. The temperature is relatively constant over the whole range of power as expected and is roughly equal to 4.2 eV. We have a pretty good confidence in the quality of the I-V characteristic fits as the mean squared error is indeed lower than 10^{-10} and the level of noise in the temperature curve is fairly low. Here, n_e seems to be much more reliable than n_i for the fit method because it depends on the exponential part of the curve for which currents are much higher compared to ion currents.

In capacitive coupling, the density plot shown in Fig. 14 exhibits almost the same values as in direct coupling for n_i, while n_e is two times lower. The temperature is constant at a low level of rf power and increases at a higher level due to the near heating effect of the electrode. The probe is not far enough (several mean free paths) to sense a pure thermal distribution of electrons, which explains the temperature rise from 5 eV to 7 eV at the highest rf power in Fig. 15.

V. RF SHEATH THICKNESS

As explained in the Introduction, measurements of the rf sheath thickness are not widespread in the plasma community. A wide panel of the potential diagnostics is presented in Ref. 18, and the conclusion is that sheaths, and especially rf sheaths, are pretty complicated to diagnose and to understand.

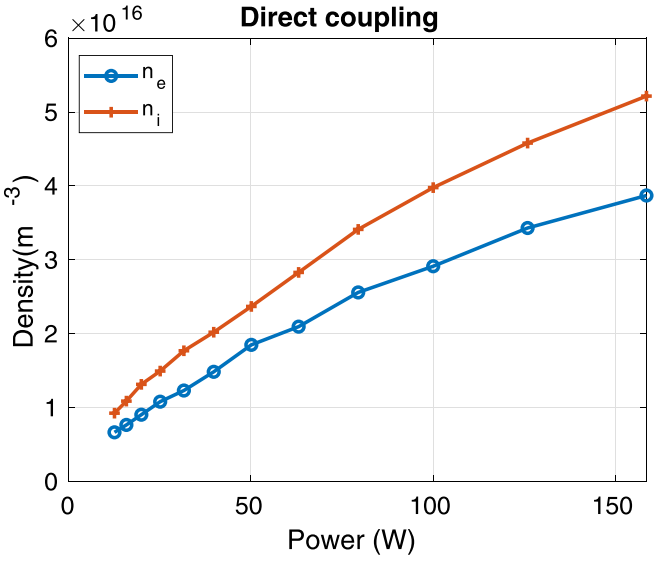

FIG. 13. Ion and electron densities from the fit method with respect to rf power in direct coupling.

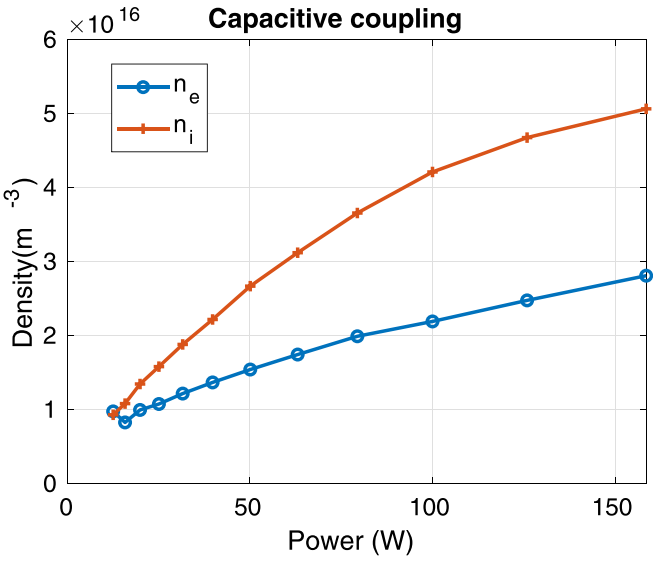

FIG. 14. Ion and electron densities from the fit method with respect to rf power in capacitive coupling.

The present technique is based on an rf compensated cylindrical Langmuir probe, thin enough (0.15 mm in diameter) to not disturb too much the potential distribution within the rf sheath. Even if the probe disturbs the equipotential lines within the sheath,[18] it does not ruin its ability to detect the sheath edge, which means that the floating potential measured is not the sheath potential but varies in the same trend as the sheath potential. That is why the Langmuir probe may be a good candidate for determining the sheath thickness.

The averaged sheath thickness can be deduced either from the potential profiles shown in Figs. 6 and 10 or from the density profiles

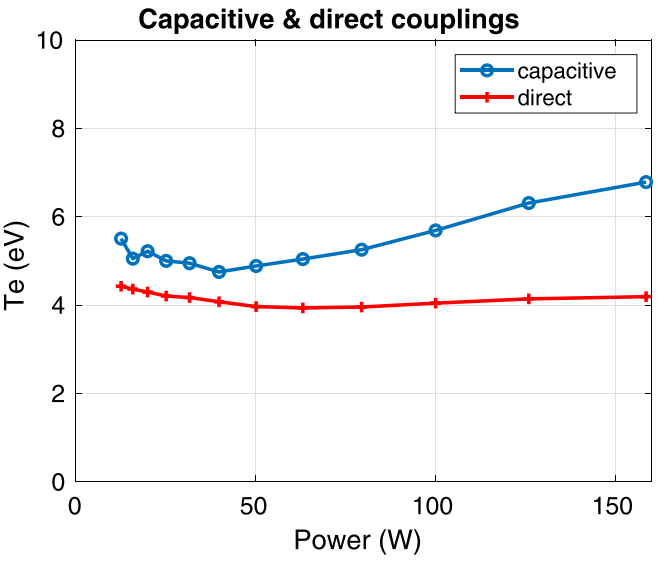

FIG. 15. Electron temperature with respect to rf power in both capacitive and direct couplings.

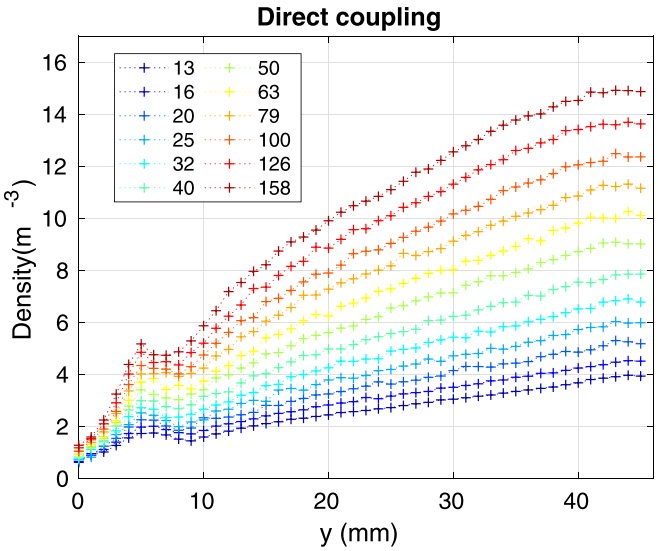

FIG. 16. Ion density profiles from the OML method with respect to the position along the y axis in direct coupling (legend: rf power in Watts).

obtained using the OML method inside the sheath. These density profiles are plotted in Figs. 16 and 17. The most astonishing thing is the accuracy of the density profiles inside the sheath. The sheath edge is then much easier to determine than in the potential profiles even if the plasma density is overestimated compared to the fit method (3 times higher). Finally, the results from both the methods can be compared.

A. Direct coupling

In direct coupling, the sheath thickness does not change much with the rf power. This is due to the increase in the density which decreases the Debye length with the rf power, which balances the total sheath expansion with the rf potential. Taking the sheath edge at the maximum of the second derivative of the potential profile (Vfl method) yields a rather constant thickness of 6 mm. But using the ion density profiles derived from the OML method and taking the position at the first maximum of density in Fig. 16, the average value for the thickness is 3.3 mm and remains almost the same for all rf power levels. The third method (Vpl method) consists in measuring the position at half the potential leap near the electrode to detect the sheath edge; as a matter of fact, the method to find out the plasma potential does not work anymore inside the sheath and its value tends to increase very quickly. In Fig. 18, the three measured thicknesses are compared with the Child–Langmuir (CL) law, Lieberman law,[8] and a semianalytical model.[11] Other experimental comparison with Godyak and Lieberman models for the electric properties of the sheath is presented in Refs. 43 and 44 for collisional and asymmetric discharges. The Godyak model[10] is rather complicated to solve and is not plotted here. But it exhibits a $V_{rf}^{\frac{1}{2}}$ dependence instead of $V_{rf}^{\frac{3}{4}}$. The Wang model is simplified by considering a factor 3 with the CL law for the same range of pressures (20–30 mTorr or 2.7–4 Pa and P = 3.5 Pa in our measurements). This model computes the sheath thickness in an argon plasma considering the slightly lower mean free path. The result for the sheath thickness does not depend on the ion mass so that one can expect the same value in a helium plasma. For the Child–Langmuir law, one assumes $\alpha = 1$, for Lieberman's law $\alpha = \sqrt{50/27}$, and $\alpha = 3$ for the Wang semianalytical model in the following expression:

$$\frac{s}{\lambda_{De}} = \alpha\left(\frac{V_{rf}}{T_e}\right)^{\frac{3}{4}} + 5, \tag{10}$$

where V_{rf} is used instead of the average potential gap in the sheath because the plasma potential V_p saturates at $V_{rf} = 80$ V due to the

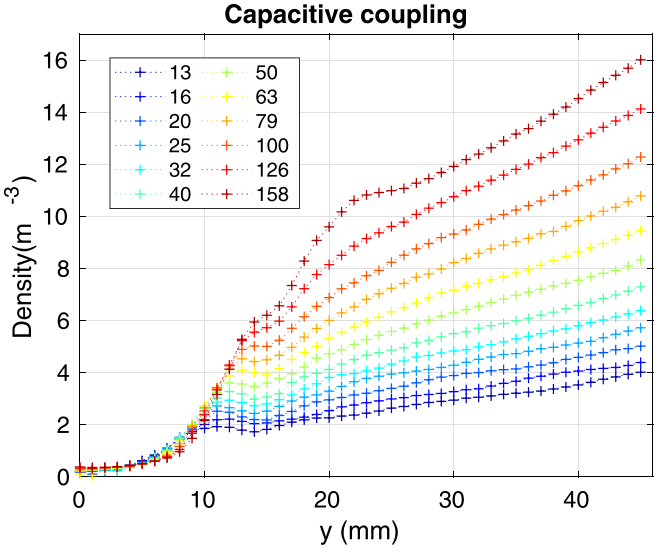

FIG. 17. Ion density profiles from the OML method with respect to the position along the y axis in capacitive coupling (legend: rf power in Watts).

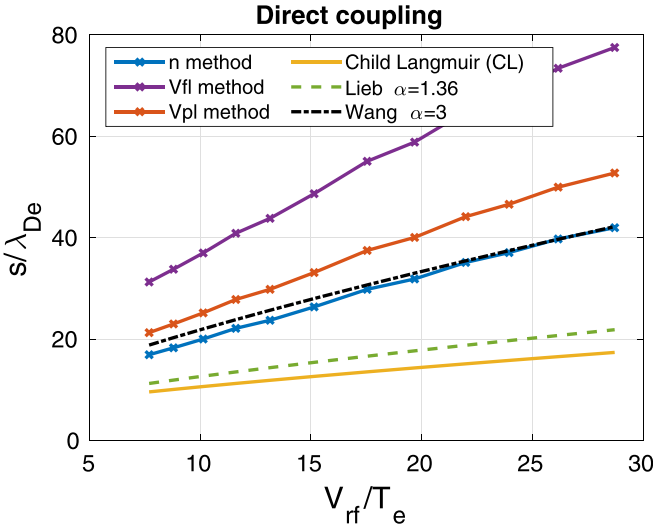

FIG. 18. Sheath thicknesses normalized to the Debye length plotted with respect to the rf potential normalized to Te in direct coupling. The 3 measured curves using the density method, the floating method, and the plasma potential method are compared with the theoretical methods (Child–Langmuir method, Lieberman method, and Wang method).

reversal of the rf sheath as seen in Fig. 9. In the same figure, the average plasma potential is almost equal to the rf potential amplitude V_{rf}, while it does not saturate. In Eq. (10), the floating sheath thickness is assumed to be equal to 5 λ_{De}.[2,7]

The sheath thickness is supposedly constant and an averaged value over all rf power is used to plot s/λ_{De}. The temperatures in Fig. 15 and the electron density n_e for direct coupling are used to calculate the Debye length. Figure 18 shows that all the measured values overestimate the theoretical sheath thicknesses as CL and Lieberman, but the "n method" measurement is finally very close to the semianalytical model ($\alpha = 3$). Other experimental methods (Vfl and Vpl methods) overestimate again all the others. The conclusion is that the real average rf sheath thickness in direct coupling is at least 3 times higher than the one given by the Child–Langmuir law in a low collisional Helium plasma.

B. Capacitive coupling

In capacitive coupling, the sheath thickness is much larger due to the matching box which enhances the negative dc biasing at the electrode V_{bias} as seen in Fig. 11. The sheath thickness is not more constant with respect to the rf power and tends to increase. So, s/λ_{De} is plotted with the deduced sheath thickness for each rf power level. Indeed, the temperature used to compute the Debye length is now the average of temperatures in Fig. 15 and the density is taken from Fig. 14 for the capacitive coupling. Looking at the sheath thickness (see Fig. 19) as a function of V_{bias}/T_e using the density method (n method) and the plasma potential method (Vpl method), one can see that both methods produced very similar results considering the uncertainties (the position accuracy is 1 mm, which means at least 10% of relative error). Again, the coefficient $\alpha = 3$, also matching the Wang's model, seems to fit well as it was the case in direct coupling. Again, CL and Lieberman laws underestimate the sheath width.

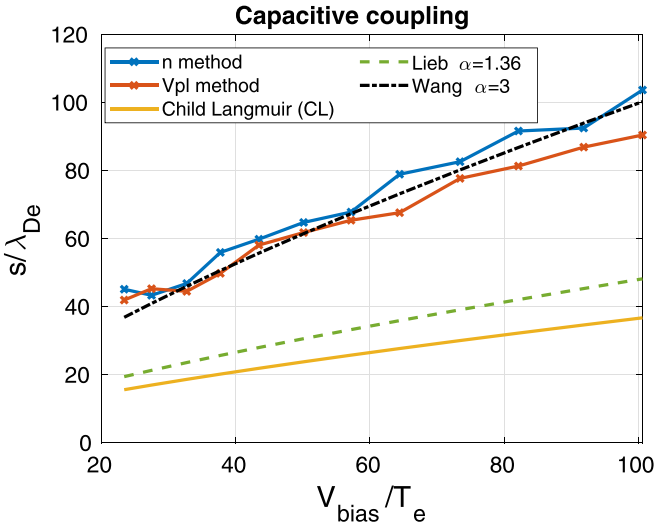

FIG. 19. Sheath thicknesses normalized to the Debye length plotted with respect to the rf potential normalized to Te in capacitive coupling. The 2 measured curves using the density method and the plasma potential method are compared with the theoretical methods (Child–Langmuir method, Lieberman method, and Wang method).

Here, the floating potential method is not plotted because it is hard to find a relevant criterion for the sheath edge. At the first sight in Fig. 10, it seems to be constant if we consider the sheath edge where the first derivative is zero, but if we plot s/λ_{De} with a constant sheath thickness, the power law is no more verified.

VI. CONCLUSION

The main goal of this work was to check the ability to make measurements within an rf sheath using an rf compensated and thin Langmuir probe in a plasma without a magnetic field. Measurements have been performed in an Aline plasma device equipped with an rf electrode and a probe mounted on a 3D manipulator to draw the potential and density profiles. The potential profiles have been plotted from the rf electrode position up to several centimeters into the core plasma. It has been shown that they are smooth enough to be analyzed, even very close to the rf electrode, inside the rf sheath. While the floating potential is easy to deduce from the I-V characteristics, the plasma potential has been extracted from the maximum of the first derivative of the characteristics using smoothing methods. The plasma potential profiles exhibit a small slope due to the presheath in the core plasma, while in the sheath, it is not reliable due to distortion of the I-V characteristics. The floating potential profiles reveal a strong decrease in the potential over the sheath edge. All these profiles allow detection of the sheath edge.

The self-biasing of the plasma due to the rf power has been checked with respect to several models in direct coupling. We found that the most adapted is a capacitive saturated model taking into account the size of each electrode. Nevertheless, this model works only under a potential threshold above which the sheath potential is reversed to allow electron acceleration. This phenomenon has been explained by the fact that the electron saturation current drained by the rf electrode is not high enough to compensate the ion current collected at the grounded wall. The higher the plasma biasing, the higher the positive current at the wall. As a consequence, the total ion current at the wall can be higher than the electron saturation current over the electrode area, and hence, a "reversed" sheath is needed in order to accelerate electrons on the electrode side. In capacitive coupling, the electrode is negatively biased so that the plasma potential remains low and weakly disturbed by rf oscillations.

The potential drop between the plasma and floating potential profiles remains constant as a function of the rf power. This potential drop has been used to compute the floating sheath thickness around the probe in the low probe voltage range ($V_p < T_e$) considering that the ion collection area is not the probe tip but the sheath edge surrounding this tip. In the present case, it yields a typical sheath thickness of 3 Debye lengths.

To compare these measured sheath thicknesses with the Child–Langmuir law at high rf potentials, the main plasma parameters (density and temperature) have been deduced from the analysis of the IV characteristics in the quasineutral plasma. This has been done using two methods, the "fit method" and the classical "OML method" for ions. The "fit method works well to find out both the ion and electron densities with relatively good agreement (less than a factor 2 between them) as well as for the electron temperature. This method does not apply anymore within the sheath due to the non-Maxwellian EEDF.

The OML theory based on the ion part of the characteristics is able to yield a continuous ion density profile from the plasma to the electrode. Even if, within the sheath, the thermal velocity is underestimated (because ions are accelerated), this method is a good way to determine the sheath edge and then its thickness.

From the comparison of the three measurement methods ("density," "plasma potential," and "floating potential" methods) with theoretical laws, the conclusion is that the density and plasma potential methods give the most reliable results, while the floating potential method seems to overestimate the sheath thickness. Nevertheless, it leads to a typical average rf sheath thickness 3 times higher than the classical Child–Langmuir law and more than 2 times higher than the Lieberman correction but in the same range as a semianalytical model given in another study. The sheath thickness law seems to be independent of the coupling for the same rf power levels. The main conclusion is that the average sheath thickness around an rf electrode is 3 times higher than the classical Child–Langmuir law, applying for relatively high dc potentials. This factor has been obtained using the amplitude of the rf potential in place of the dc potential drop in a Child–Langmuir like formula, in the case of a direct coupling. As a matter of fact, the sheath potential drop cannot be used because of the saturation of the self-biasing of the plasma, due to the sheath potential reversal at high rf power. In capacitive coupling, the real averaged potential drop in the sheath has been used.

ACKNOWLEDGMENTS

This work was carried out within the framework of the French Federation for Magnetic Fusion Studies (FR-FCM) and of the Eurofusion Consortium and received funding from the Euratom Research and Training Programme 2014–2018 and 2019–2020 under Grant Agreement No. 633053. The views and opinions expressed herein do not necessarily reflect those of the European Commission.

REFERENCES

[1]Y. P. Raizer, M. N. Shneider, and N. A. Yatsenko, *Radio-Frequency Capacitive Discharges*, 1st ed. (CRC Press, 1995).
[2]M. A. Lieberman and A. J. Lichtenberg, *Principles of Plasma Discharges and Materials Processing*, 2nd ed. (Wiley, 2005).
[3]P. Chabert and N. Braithwaite, *Physics of Radio-Frequency Plasmas* (Cambridge University Press, Cambridge, 2011).
[4]V. A. Godyak and A. A. Kuzovnikov, Fiz. Plasmy **1**, 496 (1975) [Sov. J. Plasma Phys. **1**, 276 (1975)].
[5]H. S. Butler and G. S. Kino, Phys. Fluids **6**, 1346 (1963).
[6]K.-U. Riemann, J. Phys. D: Appl. Phys. **24**, 493 (1991).
[7]P. Chabert, Plasma Sources Sci. Technol. **23**, 065042 (2014).
[8]M. A. Lieberman, IEEE Trans. Plasma Sci. **16**, 638 (1988).
[9]M. A. Lieberman, IEEE Trans. Plasma Sci. **17**, 338 (1989).
[10]V. A. Godyak and N. Sternberg, Phys. Rev. A **42**(4), 2299 (1990).
[11]S.-B. Wang and A. E. Wendt, IEEE Trans. Plasma Sci. **27**, 1358 (1999).
[12]M. A. Lieberman, J. Appl. Phys. **65**, 4186 (1989).
[13]K. Köhler, J. W. Coburn, D. E. Horne, and E. Kay, J. Appl. Phys. **57**, 59 (1985).
[14]Y. P. Raizer and M. N. Schneider, Plasma Sources Sci. Technol. **1**, 102 (1992).
[15]A. Metze, D. W. Ernie, and H. J. Oskam, J. Appl. Phys. **60**, 3081 (1986).
[16]A. M. Pointu, J. Appl. Phys. **60**, 4113 (1986).
[17]E. Faudot, Phys. Plasmas **22**, 083506 (2015).
[18]N. Hershkowitz, Phys. Plasmas **12**, 055502 (2005).
[19]L. Oksuz and N. Hershkowitz, Phys. Rev. Lett. **89**, 145001 (2002).
[20]M.-H. Cho, N. Hershkowitz, and T. Intrator, J. Vac. Sci. Technol., A **6**, 2978 (1988).
[21]S. Kajita, S. Kado, A. Okamoto, T. Shikama, Y. Iida, D. Yamasaki, and S. Tanaka, in 12th International Congress on Plasma Physics, Nice (France), 25–29 October (2004); arXiv:physics/0410187.
[22]A. H. Sato and M. A. Lieberman, J. Appl. Phys. **68**(12), 6117 (1990).
[23]H.-S. Han, H.-C. Lee, S.-J. Oh, and C.-W. Chung, Phys. Plasmas **21**, 023512 (2014).
[24]H. M. Mott-Smith and I. Langmuir, Phys. Rev. **28**, 727 (1926).
[25]J. E. Allen, R. L. F. Boyd, and P. Reynolds, Proc. Phys. Soc. (London) B **70**, 297 (1957).
[26]F. F. Chen, J. Nucl. Energy, Part. C **7**, 47 (1965).
[27]I. B. Bernstein and I. N. Rabinowitz, Phys. Fluids **2**, 112 (1959).
[28]J. G. Laframboise, Aerospace Studies Report No. 100 (University Toronto Institute, 1966).
[29]F. F. Chen, J. D. Evans, and D. Arnush, Phys. Plasmas **9**, 4 (2002).
[30]P. A. Chatterton, J. A. Reese, W. L. Wu, and K. Al Assadi, Vacuum **42**(7), 489–493 (1991).
[31]F. F. Chen, Plasma Sources Sci. Technol. **21**, 055013 (2012).
[32]E. Faudot, S. Devaux, J. Moritz, S. Heuraux, P. Molina Cabrera, and F. Brochard, Rev. Sci. Instrum. **86**, 063502 (2015).
[33]F. F. Chen, Plasma Sources Sci. Technol. **18**, 035012 (2009).
[34]D. Bohm, in *The Characteristics of Electrical Discharges in Magnetic Fields*, edited by A. Guthrie and R. K. Wakerling (McGraw-Hill, New York, 1949), p. 77.
[35]V. A. Godyak, Fiz. Plazmy **2**, 141 (1976).
[36]A. Garscadden and K. G. Emeleus, Proc. Phys. Soc. **79**, 535 (1962).
[37]J. H. Keller and W. B. Pennebaker, IBM J. Res. Dev. **23**, 3 (1979).
[38]T. D. Mantei, J. Electrochem. Soc. **130**, 1958 (1983).
[39]B. P. Wood, M. A. Lieberman, and A. J. Lichtenberg, IEEE Trans. Plasma Sci. **23**(1), 89 (1995).
[40]A. Aanesland, C. Charles, R. W. Boswell, and M. A. Lieberman, Phys. Plasmas **12**, 103505 (2005).
[41]C. Forest and N. Hershkowitz, J. Appl. Phys. **60**, 1295 (1986).
[42]M.-H. Cho, N. Hershkowitz, and T. Intrator, J. Appl. Phys. **67**, 3254 (1990).
[43]V. A. Godyak, O. A. Popov, and A. H. Hanna, in Proceedings of the XIII International Conference on Phenomena in Ionized Gases, Berlin (1977), p. 347.
[44]M. A. Sobolewski, Appl. Phys. Lett. **70**(8), 1049 (1997).
[45]S. Devaux, E. Faudot, J. Moritz, and S. Heuraux, Nucl. Mater. Energy **12**, 908 (2017).